Geometry and electronic band structure of an ordered monolayer deposition of Bi on III-V(110) semiconductor surfaces

A. Umerski* and G. P. Srivastava
Department of Physics, University of Exeter, Stocker Road, Exeter EX4 4QL, United Kingdom
(Received 9 August 1994; revised manuscript received 11 October 1994)

We present calculational studies of the electronic and geometric structure of an ordered monolayer deposition of Bi on III-V(110) surfaces. The technique which we have applied to these systems relies on the complete self-consistent solution of the Kohn-Sham equations for both the electronic and ionic degrees of freedom. An *ab initio* pseudopotential method, within the local-density approximation, is used in a supercell approach. From a given initial set of atomic positions, a conjugate-gradient technique is used to achieve the equilibrium geometry by moving along the Born-Oppenheimer subspace. The calculated relaxed geometries of the clean and Bi-covered (110) surface of GaAs, InP, and InAs compare well with available low-energy electron-diffraction and x-ray standing-wave studies, and the electronic band structures agree with angle-resolved photoemission results. The orbital nature of states that might participate in Schottky-barrier formation at Bi-covered surfaces is also discussed.

I. INTRODUCTION

At room temperature most metal adsorbates are known to react disruptively with the III-V(110) semiconductor surface.[1] However, the growth of a monolayer (1 ML) of Sb or Bi has been found to result in a stable and ordered (1×1) structure.[2] Therefore III-V(110)-Sb (1 ML) and III-V(110)-Bi (1 ML) have served as useful prototypical systems for studying both nontrivial surface geometries and Schottky barrier formation. Many experimental studies of the electronic[3–5] and structural[6–9] properties of these systems have been undertaken. Theoretical studies have so-far been limited to the clean III-V(110) surface,[11,14] III-V(110)-Sb (1 ML),[9–12] and very recently GaAs(110)-Bi(1 ML).[15] The absence of *ab initio,* parameter free, theoretical studies of atomic and electronic structure has been a hampering factor in the analysis of angle-resolved photoemission data[4,5] for Bi overlayer systems, which have proceeded by assuming a strong similarity with the Sb monolayer systems.

Proposed geometrical models for the Sb monolayer include Goddard's epitaxial continued layer structure[16] (ECLS), epitaxial on top structure,[14] relaxed Skeath's (p^3) structure,[17] and overlapping chain structure.[14] Although scanning-tunnel-microscope micrographs are unable to distinguish[18] between the ECLS and p^3 models, recent low-energy-electron-diffraction (LEED) (Refs. 6 and 7) and x-ray standing-wave (XSW) (Ref. 8) analyses, as well as *ab initio* theoretical studies, have confirmed that the correct ground-state configuration of the Sb monolayer is the Goddard's model (i.e., ECLS). The recent LEED (Refs. 6 and 7) and XSW (Ref. 9) studies have also confirmed the ECLS model for the Bi monolayer on III-V(110).

To provide a consistent and accurate study of both atomic and electronic structure of the Bi overlayer system an adequate theoretical basis is required. The principal theoretical tool for calculating structural and electronic properties of solids and surfaces in recent years has been the use of computational models employing the local approximation of the density-functional theory. Within this theory, the vast majority of effort has concentrated on the development of the molecular dynamics or Car-Parinello technique.[19] However, there is an alternative approach[20] based upon the self-consistent solution of the Kohn-Sham equations[21] for both electronic and ionic coordinates. We have recently[5] developed a reliable method for obtaining the electronic and structural properties of atomic systems within this scheme.

In this paper, we discuss some of the theoretical and technical aspects which we have developed[15] for our calculations. We start (in Sec. II A) with a brief resume of the Kohn-Sham equations within the supercell approach. We then present an overview of our method of solving these equations, for the electronic degrees of freedom (in Sec. II B), and for the geometric degrees of freedom (in Sec. II C). In Sec. III, we present the results of our calculations as applied to GaAs(110), InP(110), and InAs(110) clean surface systems and provide a comparison with existing experimental and theoretical data. In Sec. IV, we present the results of our calculations as applied to GaAs(110)-Bi(1 ML), InP(110)-Bi(1 ML), and InAs(110)-Bi(1 ML) within the Goddard geometry (the ECLS), and compare these results with any existing experimental data. We comment upon the structural trends for these systems, and their formation energies. In addition, we discuss the orbital nature of states which might be responsible for Schottky barrier formation at these interfaces.

II. METHOD

A. Kohn-Sham equations

Consider a periodic system, with a unit cell consisting of $2M$ interacting valence electrons and L ionic cores at positions $\{\mathbf{R}_I; I=1,\ldots,L\}$. According to the

Hohenberg-Kohn theorem,[21] the ground-state energy $E_0=E[n_0,\mathbf{R}]$ is a functional of the ground-state electron charge density $n_0(\mathbf{r})$. An electronic charge density $n(\mathbf{r})$ (for the spin degenerate case) is given by

$$n(\mathbf{r})=\frac{2v}{(2\pi)^3}\int_{1\mathrm{BZ}} d\mathbf{k}\sum_{i=1}^{M}|\psi_{\mathbf{k}}^i(\mathbf{r})|^2$$

$$\approx\frac{2v}{(2\pi)^3}\sum_{\mathbf{k}_\alpha} w_\alpha\sum_{i=1}^{M}|\psi_{\mathbf{k}_\alpha}^i(\mathbf{r})|^2 . \quad (2.1a)$$

Here, v is the volume of the unit cell, and the integral over the first Brillouin zone (1 BZ) in $\mathbf{K}$ space can be approximated by a finite sum over so-called special weighted $\mathbf{k}$ points $\mathbf{k}_\alpha$ with weight w_α. In the "pseudopotential" theory $\{\psi_{\mathbf{k}}^i(\mathbf{r});i=1,\ldots,M\}$ are (doubly occupied) single-particle (pseudo-) wave functions of a fictitious system, which by Bloch's theorem may be expanded in a plane wave basis set:

$$\psi_{\mathbf{k}}^i(\mathbf{r})=\sum_{\mathbf{G}} e^{i(\mathbf{k}+\mathbf{G})\cdot\mathbf{r}}\phi_{\mathbf{k}+\mathbf{G}}^i ,$$

$$\mathbf{G}\in\Re \text{ such that } |\mathbf{k}+\mathbf{G}|^2\le E_{\mathrm{cut}} , \quad (2.1b)$$

where the $\mathbf{G}$ vectors range over a ball of radius $\sqrt{E_{\mathrm{cut}}}$ (in Ry units, for some cutoff energy E_{cut}) in the reciprocal space $\Re$. In order to derive the ground-state charge density $n_0(\mathbf{r})$ from the pseudodensity $n(\mathbf{r})$, we must solve an $N_{\mathbf{k}}\times N_{\mathbf{k}}$ nonlinear matrix eigenvalue problem (the Kohn-Sham equations[21] at $\mathbf{k}$ in $\mathbf{K}$ space) for the coefficients $\{\phi_{\mathbf{k}+\mathbf{G}}^i\}$:

$$\sum_{\mathbf{G}'} H_{\mathbf{k}+\mathbf{G},\mathbf{k}+\mathbf{G}'}\phi_{\mathbf{k}+\mathbf{G}'}^i=\varepsilon^i\phi_{\mathbf{k}+\mathbf{G}}^i , \quad (2.1c)$$

and substitute the result into Eq. (2.1b) and then Eq. (2.1a). The Kohn-Sham Hamiltonian matrix,

$$\mathbf{H}(\tilde{n},\mathbf{R})=\mathbf{D}^{\mathrm{KE}}+\mathbf{V}^H(\tilde{n})+\mathbf{V}^{\mathrm{XC}}(\tilde{n})+\mathbf{V}^{\mathrm{PS}}(\mathbf{R}) , \quad (2.1d)$$

is a function only of the ionic coordinates $\mathbf{R}$, and the Fourier transform $\tilde{n}$ of the charge density n. In the pseudopotential approach and local-density approximation (LDA) $\mathbf{H}$ can be understood as a sum of physical terms: $\mathbf{D}^{\mathrm{KE}}$ is the diagonal kinetic-energy matrix; $\mathbf{V}^H$ represents the classical Coulomb (or Hartree) electron-electron energy; $\mathbf{V}^{\mathrm{XC}}$ is the electron exchange-correlation energy within the LDA; and $\mathbf{V}^{\mathrm{PS}}$ is the pseudopotential part of the Hamiltonian, representing the electron-ion Coulombic interaction. Note that the off-diagonal Hamiltonian matrix elements require consideration of reciprocal-lattice vectors up to the kinetic-energy cutoff $2\sqrt{E_{\mathrm{cut}}}$.

B. Solution of electronic degrees of freedom

For a fixed set of ionic coordinates $\mathbf{R}$, the ground-state charge density $n_0(\mathbf{r})$ must be obtained by solving the Kohn-Sham equations (2.1a) at each of the special $\mathbf{k}$ points for the ϕ's. Since, however, the Kohn-Sham equations are nonlinear (i.e., $\mathbf{H}$ is dependent upon ϕ), then for their solution one must proceed in an iterative manner. We use a "diagonalization-update" technique, in which the "update" is performed by a quasi-Newton-Raphson (Broyden's Jacobian update) method.[22] We label the "update" iterates by $\mu=1,\ldots,n_{\mathrm{up}}$. Within the "diagonalization-update" algorithm, the time and memory dominant step is that of the diagonalization. If a conventional Householder method is used, then the memory requirement per $\mathbf{k}$-point scales as $O(N_{\mathbf{k}}^2)$ and the CPU requirement as $O(N_{\mathbf{k}}^3)$. However, it is important to realize that only the lowest M eigenvalues and eigenvectors (i.e., those occupied) are required [cf. Eq. (2.1d)] to compute n_0. Hence, it is expedient to use an iterative technique which exploits this fact. We employ a semiblock RM-DIIS (residual minimization by direct inversion in interactive subspace) technique with some modifications. In order to appreciate these, let us recap the salient features of the conventional RM-DIIS method.[23]

The standard RM-DIIS algorithm to solve the $N\times N$ eigenvalue problem $\mathbf{H}|e\rangle=E|e\rangle$ begins with a best approximation $|e^{(1)}\rangle$ to $|e\rangle$ and $E^{(1)}$ to E; a (one-dimensional) vector space $\mathbf{V}^{(1)}\equiv\{|e^{(1)}\rangle\}$; a (one-dimensional) vector space $\mathbf{HV}^{(1)}\equiv\{\mathbf{H}|e^{(1)}\rangle\}$; and then proceeds iteratively (with iterates labeled by $n,r,s=1,\ldots,n_{\mathrm{DIIS}}$), so that at the beginning of the nth iteration we have a best approximation $|e^{(n)}\rangle$ to $|e\rangle$ and $E^{(n)}$ to E; a sequence of vectors $\mathbf{V}^{(n)}=\{|v^{(1)}\rangle,\ldots,|v^{(n)}\rangle\}$ (forming the iterative subspace); a second sequence of vectors $\mathbf{HV}^{(n)}=\{|\mathbf{H}v^{(1)}\rangle,\ldots,|\mathbf{H}v^{(n)}\rangle\}$. We then continue by solving the $n\times n$ generalized eigenvalue problem (the direct inversion):

$$\mathbf{Rc}=\lambda\mathbf{Sc} , \quad (2.2a)$$

where

$$\mathbf{R}_{rs}=\langle e^{(r)}|\mathbf{H}|e^{(s)}\rangle \text{ and } \mathbf{S}_{rs}=\langle e^{(r)}|e^{(s)}\rangle \quad (2.2b)$$

for the lowest eigenvalue λ, using conventional Householder diagonalization so that we obtain

$$|e^{(n+1)}\rangle=\sum_{r=1}^{n}\mathbf{c}_r|e^{(r)}\rangle \text{ and } E^{(n+1)}=\lambda . \quad (2.2c)$$

Next, we define the residual

$$|R(e^{(n+1)},E^{(n+1)})\rangle\equiv(\mathbf{H}-E^{(n+1)})|e^{(n+1)}\rangle , \quad (2.2d)$$

and, finally, we obtain

$$|v^{(n+1)}\rangle=\mathbf{A}^{(n+1)}|R(e^{(n+1)},E^{(n+1)})\rangle \quad (2.2e)$$

and

$$|\mathbf{H}v^{(n+1)}\rangle=\mathbf{H}|v^{(n+1)}\rangle \quad (2.2f)$$

for some "almost diagonal" matrix $\mathbf{A}^{(n+1)}$ (which will be discussed shortly). We may then proceed to the $(n+1)$th iteration.

In order to find the lowest M eigenvectors $[\mathbf{H}|e_i\rangle=E_i|e_i\rangle(i=1,\ldots,M)]$, we could proceed in a sequential manner as follows. First use RM-DIIS to find the lowest eigenvector $|e_1\rangle$. Then use RM-DIIS to find the next lowest eigenvalue $|e_2\rangle$ but ensuring orthogonality of $\mathbf{V}^{(r)}$ to the lowest eigenvalue $|e_1\rangle$ at each iteration r, and so on. Now, if the maximum number of iterations likely to produce a reliable eigenvector is n_{DIIS}, then the

naive theoretical computational cost of this exercise will be $O(Nn_{\mathrm{DIIS}})$ in memory and $O[M(n_{\mathrm{DIIS}}N^2+n_{\mathrm{DIIS}}^3)]$ in CPU. We use the term *naive* here, because, in practice, reading the matrix elements of $\mathbf{H}$ or calculating them takes one or two orders of magnitude longer than it takes to multiply $\mathbf{H}$ with a vector. Thus, the real CPU requirement will be $O[M(n_{\mathrm{DIIS}}\tau N^2+n_{\mathrm{DIIS}}^3)]$, where $\tau\sim 10-100$.

We avoid this congestion by using a "semi-block" technique, in which at the nth iteration we have stored our best approximations $\{|e_1^{(n)}\rangle,\ldots,|e_M^{(n)}\rangle\}$ and $\{E_1^{(n)},\ldots,E_M^{(n)}\}$ to the M lowest eigenvectors and eigenvalues $\{|e_1\rangle,\ldots,|e_M\rangle\}$ and $\{E_1,\ldots,E_M\}$; M sequences of n vectors $\{\mathbf{V}_1^{(n)},\ldots,\mathbf{V}_M^{(n)}\}$, where $\mathbf{V}_i^{(n)}=\{|v_i^{(1)}\rangle,\ldots,|v_i^{(n)}\rangle\}$ $(i=1,\ldots,M)$; M sequences of n vectors $\{\mathbf{HV}_1^{(n)},\ldots,\mathbf{HV}_M^{(n)}\}$, where $\mathbf{HV}_i^{(n)}=\{|Hv_i^{(1)}\rangle,\ldots,|Hv_i^{(n)}\rangle\}$ with $i=1,\ldots,M$. The idea here being that each of the $\mathbf{V}_i^{(n)}$ forms the iterative subspace for the ith lowest eigenvector. In addition, the sequences of vectors are required to satisfy $\langle e_i^{(n)}|v_j^{(r)}\rangle=\delta_{ij}$ for all $r=1,\ldots,n$ and $i,j=1,\ldots,M$ (i.e., we are demanding that $|e_i^{(n)}\rangle$ is perpendicular to $\mathbf{V}_j^{(n)}$ for $j\neq i$). We then proceed as in the regular RM-DIIS case and diagonalize each of the $n\times n$ generalized eigenvalue problems formed within $\mathbf{V}_j^{(n)}$. We are thus able to calculate $\{|e_1^{(n+1)}\rangle,\ldots,|e_M^{(n+1)}\rangle\}$, $\{E_1^{(n+1)},\ldots,E_M^{(n+1)}\}$, and $\{|v_1^{(n+1)}\rangle,\ldots,|v_M^{(n+1)}\rangle\}$. It is now possible to obtain $\{|\mathbf{H}v_1^{(n+1)}\rangle,\ldots,|\mathbf{H}v_M^{(n+1)}\rangle\}$ by using only a single call to each of the matrix elements of $\mathbf{H}$. Thus, the calculational cost of this technique is $O(n_{\mathrm{DISS}}NM)$ in memory, but only $O[M(n_{\mathrm{DIIS}}N^2+n_{\mathrm{DIIS}}^3)]$ in CPU (i.e., we sacrifice an order M in memory for a gain of one or two orders of magnitude in CPU).

This technique should be contrasted with the full-block RM-DIIS algorithm,[23] in which the iterative subspace used at the nth iteration is $\mathfrak{R}^{(n)}\cong\mathbf{V}_1^{(n)}\times\cdots\times\mathbf{V}_M^{(n)}$ — of dimension Mn. This yields the same memory requirements as the semiblock method, but the diagonalization now occurs over the whole of $\mathfrak{R}^{(n)}$, so that the CPU cost is $O(Mn_{\mathrm{DIIS}}N^2+(n_{\mathrm{DIIS}}M)^3)$. If the number of iterations n_{DIIS} required to achieve convergence is large, then the second term in this sum quickly becomes dominant. One might imagine that the increased dimension of the iterative subspace leads to a much smaller value of n_{DIIS} here. However, in practice, we have found that the number n_{DIIS} of iterations required for the semiblock diagonalization is only very slightly larger ($\leq 5\%$) than the number required in the block case, so that we always find the semiblock technique to be superior.

Our algorithm is initiated by choosing the sets $\{|e_1^{(1)}\rangle,\ldots,|e_M^{(1)}\rangle\}$ and $\{E_1^{(1)},\ldots,E_M^{(1)}\}$ as close to the exact eigenvalues and eigenvectors as possible. This is achieved by a combination of two methods.

(i) For the first few iterations (i.e., $\mu=1$ or 2) in the electronic "update" cycle, we use a Löwdin first-order perturbation type approach, in which a $Q\times Q$ $(Q\ll N; Q\geq M)$ submatrix $\mathbf{G}$ of $\mathbf{H}$ is chosen (normally so that the diagonals of $\mathbf{G}$ contain the Q smallest diagonal terms in $\mathbf{H}$) and diagonalized.

(ii) For the remaining iterations ($\mu\geq 2$) in the electronic "update" algorithm, the $\{|e_i^{(1)}\rangle\}$ are chosen as the exactly calculated eigenvectors $\{|e_i\rangle\}$ obtained[24] from the previous iteration, i.e., $(\mu-1)$th iteration.

The accelerator or preconditioning[25] matrix $\mathbf{A}^{(n+1)}$ in Eq. (2.2e) is required to accelerate the convergence of the iterative subspace. Thus, we wish to choose it so that (a) the residual $|R(e^{(n+1)}+v^{(n+1)},E^{(n+1)})\rangle$ vanishes or nearly vanishes, and that (b) $\mathbf{A}^{(n+1)}|R(e^{(n+1)},E^{(n+1)})\rangle$ be easily calculable. Condition (a) is satisfied exactly if $\mathbf{A}^{(n+1)}=(\mathbf{H}-E)^{-1}$, so that if $B=\{|b_i\rangle;i=1,\ldots,N\}$ is a complete orthonormal basis, then $\mathbf{A}^{(n+1)}$ can be approximated by[23]

$$\mathbf{A}^{(n+1)}\approx\sum_{i=1}^{N}{}'\frac{|b_{i'}\rangle\langle b_i|}{\langle b_i|\mathbf{H}-E^{(n+1)}|b_i\rangle}\ , \tag{2.2g}$$

where the prime denotes the omission of any terms where the denominator is very small. The formula is exact for the case $|b_i\rangle=|e_i\rangle$, and correspondingly more precise the closer the set B to the $\{|e_i\rangle\}$. Wood and Zunger,[23] therefore, suggested using the basis obtained from the initialization procedure [i.e., (i) as described above]. We have found that if the number of eigenvectors (M) being calculated is reasonably high, then (at iteration n) an improved preconditioning matrix $\mathbf{A}^{(n+1)}$ can be obtained by replacing the M lowest vectors of B by the current best estimates for the eigenvectors $\{|e_i^{(n+1)}\rangle\}$ (even though the resulting basis is not completely orthogonal). For the systems considered in this paper, we have $M/N\sim 50/1500$ so that we are diagonalizing about 3% of the total vector space. We find that our improved preconditioning algorithm reduces the amount of time spent performing the diagonalization by a factor of 2–4 over that used by Wood and Zunger.

C. Solution to geometric degrees of freedom

For a given ionic configuration $\mathbf{R}$, once the solution $\{\psi_{0\mathbf{k}}^i(\mathbf{r})\}$ to the Kohn-Sham equations has been calculated, the ground-state charge density $n_0(\mathbf{r})$ may be determined using Eq. (2.1a) and the total energy $E[n_0,\mathbf{R}]$ may be evaluated using momentum space formulation.[26,27] Then within the plane-wave basis, the Hellmann-Feynman forces $\mathbf{F}[n_0,\mathbf{R}]$ given by

$$F_I[n_0,\mathbf{R}]=-(\nabla E)_I=-\frac{dE[n_0,\mathbf{R}]}{dR_I} \tag{2.3a}$$

can also be computed straightforwardly in the momentum space formulation.[26,27] In order to find the equilibrium atomic structure, we, therefore, need to solve the $3L$ dimensional equation,

$$\mathbf{F}[n_0,\mathbf{R}]=\mathbf{0} \tag{2.3b}$$

for $\mathbf{R}$. Since this equation is highly nonlinear, it is necessary to pursue an iterative solution. The principal methods for solving such equations are the "one-dimensional minimization techniques".[28,29] These deduce the solution $\mathbf{R}_0$ to Eq. (2.3a) by finding the minimum of the ground-state energy $E[n_0,\mathbf{R}]$. This pro-

cedure is as follows.

Let us label the iterations in this process by Σ, $\Omega=1,\ldots,n_{\text{geom}}$. Then at the Ωth iteration, we have calculated an atomic configuration $\mathbf{R}^{\Omega}$ (our best approximation to $\mathbf{R}_0$), the total energy $E[n_0,\mathbf{R}^{\Omega}]$, and the Hellmann-Feynman forces $F[n_0,\mathbf{R}^{\Omega}]$. Then to proceed to the $(\Omega+1)$th iteration, we (i) choose a direction $\mathbf{d}^{\Omega}$; (ii) find the solution t_0 which minimizes $E[n_0,\mathbf{R}^{\Omega}+\mathbf{d}^{\Omega}t]$ (i.e., a one-dimensional minimization in the direction $\mathbf{d}^{\Omega}$); (iii) set $\mathbf{R}^{\Omega+1}=\mathbf{R}^{\Omega}+\mathbf{d}^{\Omega}t_0$ and calculate $E[n_0,\mathbf{R}^{\Omega+1}]$, $F[n_0,\mathbf{R}^{\Omega+1}]$.

Within this algorithm there are two points which need to be addressed.

(a) How is the direction $\mathbf{d}$ chosen? For the first iteration, we have the obvious choice $\mathbf{d}=-\mathbf{F}[n_0,\mathbf{R}]$. If we maintained this choice at all the iterates for the equilibrium geometry, then we would be using the so-called "steepest-decent" technique. This method, however, is not very efficient at providing a converged solution. We find that a far more efficient method, which requires minimal storage, and proves very robust, is provided by the *conjugate-gradient method*. This technique is specifically designed for the quadratic problem $[E(\mathbf{x})=a+\mathbf{bx}+\mathbf{x}^{\mathrm{T}}\mathbf{Cx}]$, where the directions $\{\mathbf{d}^{\Omega}\}$ (for iterations $\Omega=1,2,\ldots,n_{\text{geom}}$) are chosen to be "conjugate" to one another [i.e., $(\mathbf{d}^{\Omega})^{T}\mathbf{C}\mathbf{d}^{\Sigma}\propto\delta^{\Omega\Sigma}$]. The precise form for $\mathbf{d}^{\Omega}$ in (ii) is dependent upon the algorithm implemented (Fletcher-Reeves, Polak-Ribiere, etc.—see Ref. 29). However, it is always chosen as a perturbation on $\mathbf{F}(\mathbf{R}^{\Omega})$, of the form

$$\mathbf{d}^{\Omega}=-\mathbf{F}(\mathbf{R}^{\Omega})+\sum_{\Sigma=0}^{\Omega-1}\gamma_{\Sigma}\mathbf{d}^{\Sigma} \tag{2.3c}$$

for some constants γ. Despite the fact that the energy function $E[n_0,\mathbf{R}]$ from density-functional theory is not quadratic in $\mathbf{R}$, however, we still find that this algorithm is robust and its application gives excellent convergence to the equilibrium configuration $\mathbf{R}_0$ in less than L iterations.

(b) How is the one-dimensional minimization performed? The conventional method to use is that due to Brent.[29] However, this routine is highly extravagant in the number of calls it makes to the function to be minimized [$E(\mathbf{R})$ in this case], which is *the* time dominant step in a computer program using the density-functional scheme. In our procedure, having arrived at the ith iteration in the algorithm with the results for $E(\mathbf{R})$ and $\mathbf{F}(\mathbf{R})$ available, we calculate $E(\mathbf{R}+\sigma\mathbf{d})$ and $\mathbf{F}(\mathbf{R}+\sigma\mathbf{d})$ (for some small increment σ), and estimate the position of the minimum t_0 by fitting a polynomial of order 3 or greater. We attempt to fit a fourth-order polynomial of positive definite second derivative, or failing this a fourth-order polynomial with a single minimum and maximal second derivative. Such fits are always unique and have the advantage over third-order polynomials of being bounded from below.

The choice of σ can be of some importance in the deduction of an accurate value for the energy minimum in a minimal number of steps (i.e., a bad choice of σ leads to a poor polynomial fit to the actual energy, and hence to a bad estimate of the true value of the energy minimum). If we approximate the energy $E(\mathbf{R})$ by a quadratic function of $\mathbf{R}$ [say $E'(\mathbf{R})=a+\mathbf{bR}+1/2\mathbf{R}^{\mathrm{T}}\mathbf{CR}$] then the minimum of E' in the direction $\mathbf{d}$ is given by

$$\mathbf{P}_0=\mathbf{R}+s_0\mathbf{d}\quad\text{where } s_0=\frac{\mathbf{bd}+\mathbf{RCd}}{\mathbf{dCd}} \tag{2.3d}$$

and a prudent choice for σ would be $\sigma=s_0$. However, in order to evaluate the expression in Eq. (2.3d), we would need a good approximation to the Hessian matrix $\mathbf{C}$. In our technique, this is obtained by using the Broyden-Fletcher-Goldfarb-Shanno Hessian update formula,[29] with $\mathbf{C}$ initialized by running the program on a relatively low (reciprocal space) cutoff energy $E_{\text{cut}}=2$ Ry. We find that this gives an improvement in performance of approximately 25% over that obtained by using a scalar update approximation to the Hessian.

Finally, having calculated $E(\mathbf{R})$ and $E(\mathbf{R}+\sigma\mathbf{d})$ and evaluated t_0, one can use the Kohn-Sham self-consistent wave functions $\psi_0(\mathbf{R})$ and $\psi_0(\mathbf{R}+\sigma\mathbf{d})$ to evaluate the initial trial wave function to $\psi_0(\mathbf{R}+t_0\mathbf{d})$ via[30]

$$\psi_0(\mathbf{R}+t_0\mathbf{d})\sim\psi_0(\mathbf{R})+t_0/\sigma[\psi_0(\mathbf{R}+\sigma\mathbf{d})-\psi_0(\mathbf{R})]\ . \tag{2.3e}$$

This gives an excellent approximation to the actual self-consistent wave function (especially when $\mathbf{R}$ or $\mathbf{R}+\sigma\mathbf{d}$ are close to $\mathbf{R}+t_0\mathbf{d}$), and leads to an overall increase in performance of about 70% over that obtained by say a good analytic initial approximation.

III. APPLICATION TO SURFACE GEOMETRY

A. Physical and calculational approximations

We simulated an isolated material surface within the supercell framework by choosing a unit cell to consist of a sandwich of vacuum and material and vacuum. The unit cells for the systems under consideration here were orthorhombic (point symmetry group C_{2v}) with volumes 16 times that of the bulk primitive (III-V) unit cell. In particular, for clean III-V(110) surface systems, we chose an atomic constituent of $\mathrm{III_9V_9}$ arranged in a slab of nine layers of III-V, while for the overlayer systems III-V(110)-Bi(1 ML) (III-V = GaAs, InP, or InAs) we chose an atomic constituent of $\mathrm{III_7V_7Bi_4}$, arranged in a slab of seven layers of III-V, with two layers of overlayer (one on either side of the III-V slab). This gave a vacuum region equivalent to seven atomic layers for both clean and covered systems.

The starting surface or interface geometries (with which the calculation is initialized) were simply taken as the continuation of the perfect III-V bulk crystal,[31] with an experimental cubic lattice constant of $a=5.653$, 5.869, and 6.058 Å for GaAs, InP, and InAs, respectively.[32] Initial mean forces per atom were of the order 0.8 eV/Å (with a maximum force of 7.0 eV/Å) in magnitude. Relaxation was performed on all the atoms in the unit cell, and was stopped when the mean force per atom dropped below 0.04 eV/Å (leaving a maximum force on any atom of 0.15 eV/Å). Typically this required 8–12 geometry iterations.

The electron-ion interaction was considered in terms of the *ab initio* norm-conserving pseudopotentials of Bachelet, Hamann, and Schlüter,[33] including angular-momentum components up to $l=2$ for the ions making up the semiconductor slab, and up to $l=3$ for Bi ions (the spin-orbit interaction being ignored). The electron-electron interactions were treated using the correlation scheme of Ceperley and Alder[34] within the local density approximation. The single-particle (electron) wave function was expanded in plane waves, up to a maximum kinetic-energy cutoff of $E_{\text{cut}}=10$ Ry. This gave a typical value for $N_{\mathbf{k}}$ of about 3000. Diagonalization of this large Hamiltonian matrix was assisted by exploiting the z-reflection symmetry present in the unit cell with the chosen odd number of atomic layers, and was performed by our "semiblock" RM-DIIS technique. The **k**-space summations were performed by considering four special points in the irreducible segment of the surface Brillouin zone.[35]

In the following discussion we have used the convention that $z\,(y)$ refers to the [110] ([001]) direction, while $\parallel$ and $\perp$ refer to the parallel and perpendicular directions of the overlayer-substrate layer atomic bonds. Atoms on the surface will be designated "surface layer," whereas atoms on the layer immediately beneath will be designated "subsurface layer" and "first substrate layer" for the clean and covered systems, respectively.

B. Results of calculations for clean systems

In Fig. 1, we have a schematic diagram of the (relaxed) top three layers of our slab systems, indicating the key LEED structural parameters. Anions represent type-V atoms, while cations represent type III. Our calculated structural parameters for these systems are presented in Table I together with any available relevant theoretical or experimental data. We observe that our calculated equilibrium geometry is close to that predicted by LEED analysis,[6,7,36] and a combination of XSW and surface-extended x-ray-adsorption fine-structure (SEXAFS) determination.[37] In addition, it is pleasing to note that we also find excellent agreement with previous Car-Parrinello type calculations.[10] This gives us strong confidence in the accuracy of our results both for the clean surfaces and the Bi overlayer systems studied here. It is interesting to note that the equilibrium geometries obtained here are relatively insensitive to starting conditions. In particular, if the LEED geometry is chosen as our starting configuration, then we obtain an identical equilibrium geometry to that obtained above. This indicates that our geometry optimization algorithm is strongly stable.

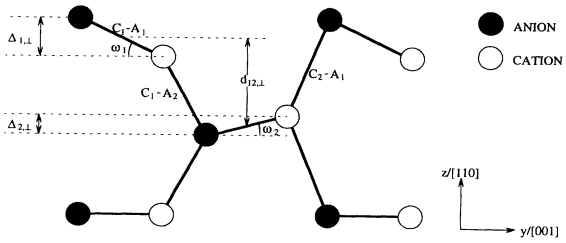

FIG. 1. Schematic representation of relaxed surface-atomic positions indicating the key structural parameters. For III-V(110)-Bi(1 ML), both anions and cations represent Bi atoms in the top layer, while in the lower layers cations (anions) represent III(V) atoms.

Figure 2 shows our calculated surface electronic states (dashed lines) for the clean surface systems superimposed on that of the bulk (continuous lines). Also shown are the experimentally derived data (open circles) from photoemission studies on GaAs(110),[38] on InP(110),[39] and on InAs(110).[40] Our anion and cation derived states are labeled A_i and C_i, respectively. In each case, we have identified four anion derived states and three cation derived states. The orbital characters of these states have been discussed in many previous papers.[10,11] However, in order for the comparison to be made with the Bi adsorbate layer, we have depicted the orbital characters of the three occupied states (A_3-A_5) and the unoccupied state (C_3) in Fig. 3. Our bands match those measured experi-

TABLE I. Calculated and experimentally derived structural parameters for III-V(110). All distances in Å, all angles in degrees.

	ω_1	ω_2	$\Delta_{1,\perp}$	$\Delta_{2,\perp}$	$d_{12,\perp}$	C_2-A_1	C_1-A_1	C_1-A_2
				GaAs(110)				
Present	30.2°	3.9°	0.66	0.09	1.75	2.42	2.40	2.34
LEED (Ref. 6)	28.4°	3.4°	0.70	0.08	1.84	2.42	2.48	2.38
Ref. 11	29°	3.8°	0.652	0.094	1.84	2.43	2.38	2.37
				InP(110)				
Present	27.1°	3.1°	0.60	0.079	1.85	2.50	2.46	2.48
LEED (Ref. 7)	31.1°	0.5°			1.88	2.55	2.52	2.49
SEXAFS (Ref. 36)	27°						2.54	
Ref. 11	29.5°	4.6°	0.67	0.11	1.93	2.46	2.42	2.42
				InAs(110)				
Present	28.7°	3.40°	0.66	0.09	1.89	2.58	2.55	2.54
LEED (Ref. 35)	31.0°		0.78	1.40	1.95	2.50	2.67	
Ref. 10	32°		0.75	0.13	1.88	2.51	2.53	

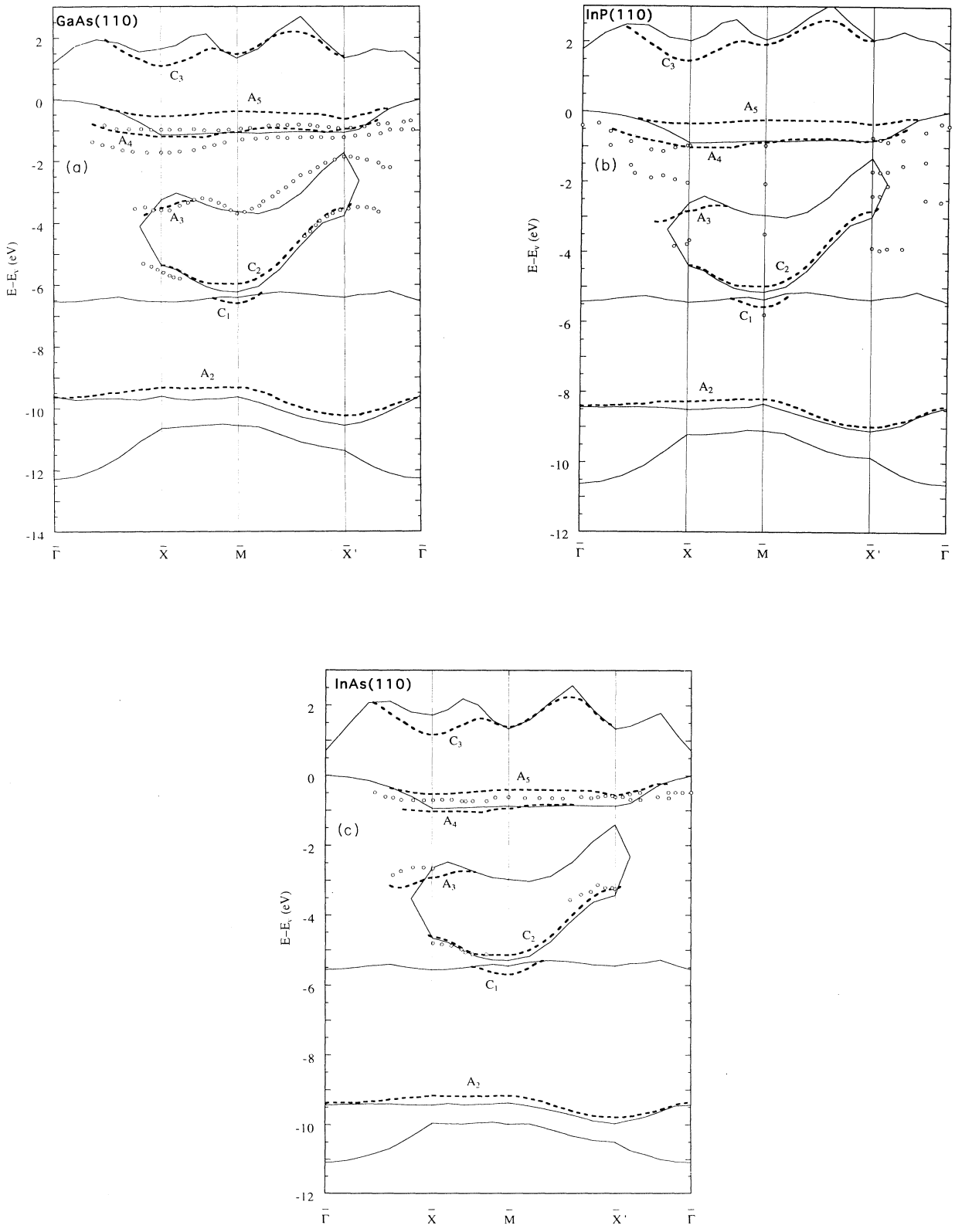

FIG. 2. Electronic band structure of clean III-V(110) surfaces: (a) GaAs(110), (b) InP(110), (c) InAs(110). Dashed lines indicate our calculated energy levels, superimposed on to projected bulk bands regions shown by solid lines, while angle-resolved photoemission results are indicated by open circles.

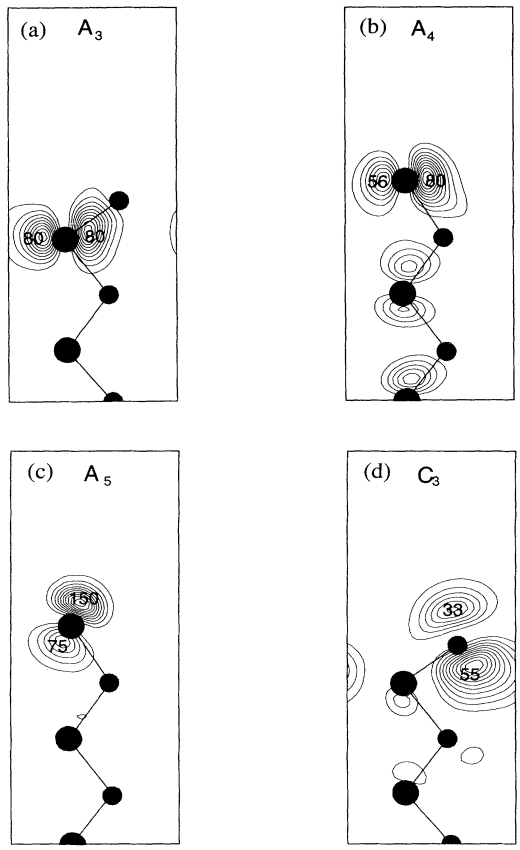

FIG. 3. Charge-density plots, in the $(1\bar{1}0)$ plane, for selected surface states on InAs(110): (a) A_3 at $\bar{X}$, (b) A_4 at $\bar{M}$, (c) A_5 at $\bar{X}$, (d) C_3 for InAs(110) at $\bar{X}$.

mentally extremely well in dispersion, and (to a lessor extent) in their energy location. In general, we find the A_5 state lies closer to the top of the bulk valence-band edge than suggested by experiment. We expect that, in agreement with the work of Alves, Hebenstreit, and Scheffler[10] use of a sufficiently large energy cutoff will shift this state down in energy, thus providing improved agreement with experiment.

Recently, Swanson *et al.*[40] have noted that their photoemission data for the A_5 state on InAs(110) agree exceptionally well with the earlier pseudopotential calculation by Alves, Hebenstreit, and Scheffler[10] within the local-density approximation. However, a significant difference between experiment and theory has been observed for the energy location of the A_3 and C_2 states. The theoretical work of Alves, Hebenstreit, and Scheffler[10] clearly suggests that the energy position of these states is not very sensitive to the size of the basis set. In view of this observation, Swanson *et al.* suggest that the experimentally measured A_3 and C_2 states could be used to provide a stringent test of quasiparticle surface band-structure calculations.[41] We do not fully agree with this suggestion, for two reasons. First, our theoretical calculations show respectable agreement with their experiment, both for A_3 and C_2. Second, it should be noted that while our calculations have been performed at the experimental lattice constant, the surface bands in the work of Alves *et al.* have been calculated at their theoretical lattice constant. The theoretical lattice constant, being approximately 2% smaller than experiment, alters the energy locations of bulk as well as surface states. Clear evidence of this is borne out from the unreasonably large bulk band gap for InAs in the calculation of Alves, Hebenstreit, and Scheffler.[10] It can be seen in Fig. 2(c) that for InAs(110) surface our theoretical results show a convincingly good overall agreement with the photoemission data of Swanson *et al.* The first unoccupied surface energy level, C_3, is found to lie at energies 1.1, 1.5, and 1.2 eV above the bulk valence-band edge for GaAs(110), InP(110), and InAs(110), respectively.[42] Consequently, this state lies just below the bulk conduction-band edge in GaAs and InP, but well above it in InAs.

Our theoretical estimates of surface-state gaps cannot be directly compared with experimental measurements, due to the modest basis set used and the band-gap problem within the local-density approximation. However, as quasiparticle calculations[41] suggest a fairly uniform shift of unoccupied states, our theoretical results can be used to investigate band-gap trends at different **k** points in the Brillouin zone. The calculated trend for the energy band gap between highest occupied and lowest unoccupied surface state at $\bar{X}$, $\bar{M}$, and $\bar{X}'$ points is $\Delta E(\bar{X}) < \Delta E(\bar{M}) < \Delta E(\bar{X}')$. This is in contrast to $\Delta E(\bar{X}') < \Delta E(\bar{X}) < \Delta E(\bar{M})$ as measured by Carstensen *et al.*[43] using a combination of direct and inverse photoemission techniques.

From the results in Table I we can make a few observations on structural characteristics of clean cleaved III-V(110) surfaces. First, since the lengths C_1-A_1, C_2-A_1, and C_1-A_2 are all similar and within about 4% of the bulk bond length, it is clear that the concept of conservation of Pauling's tetrahedral radii is maintained at these surfaces (i.e., the surface atoms are "free" to move in the direction perpendicular to the surface, and, therefore, settle at positions in accordance with their Pauling radii). Second, in all the three cases studied here, we find that the top atomic layer of these clean surfaces have moved towards the bulk (i.e., $d_{12,\perp}$ is smaller than the bulk interplanar distance along [110], by about 10%). Third, the clean cleaved III-V(110) surface layer shows a characteristic tilt angle ω_1 in the range 27°–30°. Anions (group-V atoms) move out of the surface plane "preferring" a pyramidal bonding geometry, and cations (group-III atoms) move into the substrate "preferring" a planar bonding geometry.

Our results, for both structure and electronic states, are in general agreement with the previously reported ab initio work,[10,11] although when making detailed comparisons it should be remembered that our work is based on experimental lattice constants, while the calculations in Refs. 8 and 9 are based on those derived from theory.

C. Results of calculations for Bi overlayer systems

In Fig. 1, we have a schematic diagram of the (relaxed) top three layers of our slab systems, indicating the key

LEED structural parameters. For III-V(110)-Bi(1 ML), both anions and cations represent the Bi atoms in the surface layer, while in the lower layers cations (anions) represent atoms from group III (V). Our calculated structural parameters for these systems are presented in Table II, together with any available experimental data.

Previous theoretical studies[11–13] of a monolayer growth of Sb on III-V(110) have considered many possible overlayer geometries. These studies have concluded, in agreement with LEED studies,[6,7] that Goddard's epitaxial continued layer structure (ECLS) is the lowest-energy configuration. The *ab initio* works in Refs. 11 and 12 have predicted that total energy of the so-called "epitaxial on top structure" is higher than the total energy of the Goddard structure by only about 0.25 eV per Sb atom. In this study, we find that the total energy of the Bi covered surfaces in the epitaxial-on-top structure is also only about 0.25 eV per Bi atom higher than that for the Goddard structure. It is also of interest to estimate the absorption energy of the Bi overlayer in the Goddard structure. With respect to the relaxed surfaces, we have calculated an upper bound for the absorption energy with the following values (in eV per Bi atom): 4.5, 4.9, and 4.8 for Bi/GaAs, Bi/InP, and Bi/InAs, respectively. (These values were obtained by calculating an upper bound for the pseudoatomic energy for Bi at the same kinetic-energy cutoff, viz. 10 Ry.)

There is good agreement between our calculated structural results and that available by LEED (Refs. 6 and 7) and x-ray standing-wave (XSW) (Ref. 9) analyses, on the Goddard geometry, for GaAs(110)-Bi(1 ML) and InP(110)-Bi(1 ML). There appears to be no available experimental data for the InAs(110)-Bi(1 ML) structure. In agreement with previous *ab initio* studies[11,12] of GaAs(110)-Sb(1 ML), we find that a monolayer adsorption of Bi on III-V(110) practically removes the surface tilt angle, and there is only a small vertical shear between inequivalent Bi atoms. For the covered systems, the Bi atoms can adopt either an anion- or cation-type behavior depending on their first substrate neighbor, and our observation of the tilt angle is in accordance with this principle—although to a much lesser extent than on clean surfaces. Low-energy-electron-diffraction,[6] STM,[4] and photoemission[4] results have also indicated two distinct and equally populated Bi sites on GaAs(110).

It is interesting to observe from Table II that the Bi-Bi bond length is almost preserved, and is close to twice Pauling's tetrahedral radius for Bi ($r=1.46$ Å). Similarly, the Bi-Ga bond length is also close to the sum of the tetrahedral radii of Bi and Ga. Furthermore, for both InAs(110) and GaAs(110) substrates, the Bi-As bond length is close to the sum of the Bi and As radii. The same is observed for the Bi-In bond length on the InP(110) and InAs(110) substrates. These observations thus vindicate the concept of bond-length conservation for the overlayer systems, a point already made for clean surfaces.

Figures 4(a), 4(b), and 4(c) show surface induced electronic states (dashed lines) for our Bi covered surface systems superimposed onto the projected bulk bands (continuous lines). Also shown (using open circles) are the experimentally derived data for GaAs(110)-Bi(1 ML),[4] InP(110)-Bi(1 M),[44] and InAs(110)-Bi(1 ML).[45] We have been able to identify a total of nine surface induced states, labeled $S_1, S_2, \ldots, S_9$. The characters of these states are quite different from those on the clean surface, which will become clear upon comparison of Figs. 3 and 5. We now discuss the overlayer states in some detail.

The lowest-energy valence state S_1 is observed in each of our three systems, and lies entirely below the bottom of the ionicity band. This state is derived from a $ss\sigma$-type bonding between the s-type wave functions located on the surface cation Bi atom and its neighboring (first substrate) anion atom [shown in Fig. 5(a) for the case of InAs(110)-Bi(1 ML) at $\bar{X}$]. The band S_2 is only observed for the cases GaAs(110)-Bi(1 ML) and InAs(110)-Bi(1 ML). It lies just above the ionicity band, and is predominantly derived from an s orbital located in the anion Bi atom. For the case of InAs(110)-Bi(1 ML) at $\bar{X}$, this state is found to be resonant with bulk s bands [see Fig. 5(b)]. The state S_3 is seen for all our overlayer systems lying high in the ionicity gap, and is associated with antibonding between the s orbitals located on the cation Bi atom and its neighboring first substrate layer anion atom [see Fig. 5(c) for the case of InAs(110)-Bi(1 ML) at $\bar{X}$]. Thus, the states S_1 and S_3 result from the bonding and anti-

TABLE II. Calculated and experimentally derived structural parameters for III-V(110)-Bi(1 ML). All distances in Å, all angles in degrees.

	ω_1	ω_2	$\Delta_{1,\perp}$	$\Delta_{2,\perp}$	$d_{12,\perp}$	C_2-A_1	C_1-A_1	C_1-A_2
				GaAs(110)-Bi (1 ML)				
Present	4.5°	7.1°	0.16	0.17	2.38	2.64	2.89	2.61
XSW (Ref. 9)			0.14±0.1		2.5±0.08		2.85±0.17	
LEED (Ref. 6)	2.6°	4.3°	0.09	0.11	2.52	2.73	2.87	2.77
				InP(110)-Bi (1 ML)				
Present	5.5°	4.1°	0.20	0.098	2.41	2.83	2.94	2.58
LEED (Ref. 7)	5.4°	1.5°			2.48	2.88	2.98	2.58
				InAs(110)-Bi (1 ML)				
Present	4.3°	5.2°	0.15	0.13	2.43	2.85	2.98	2.67

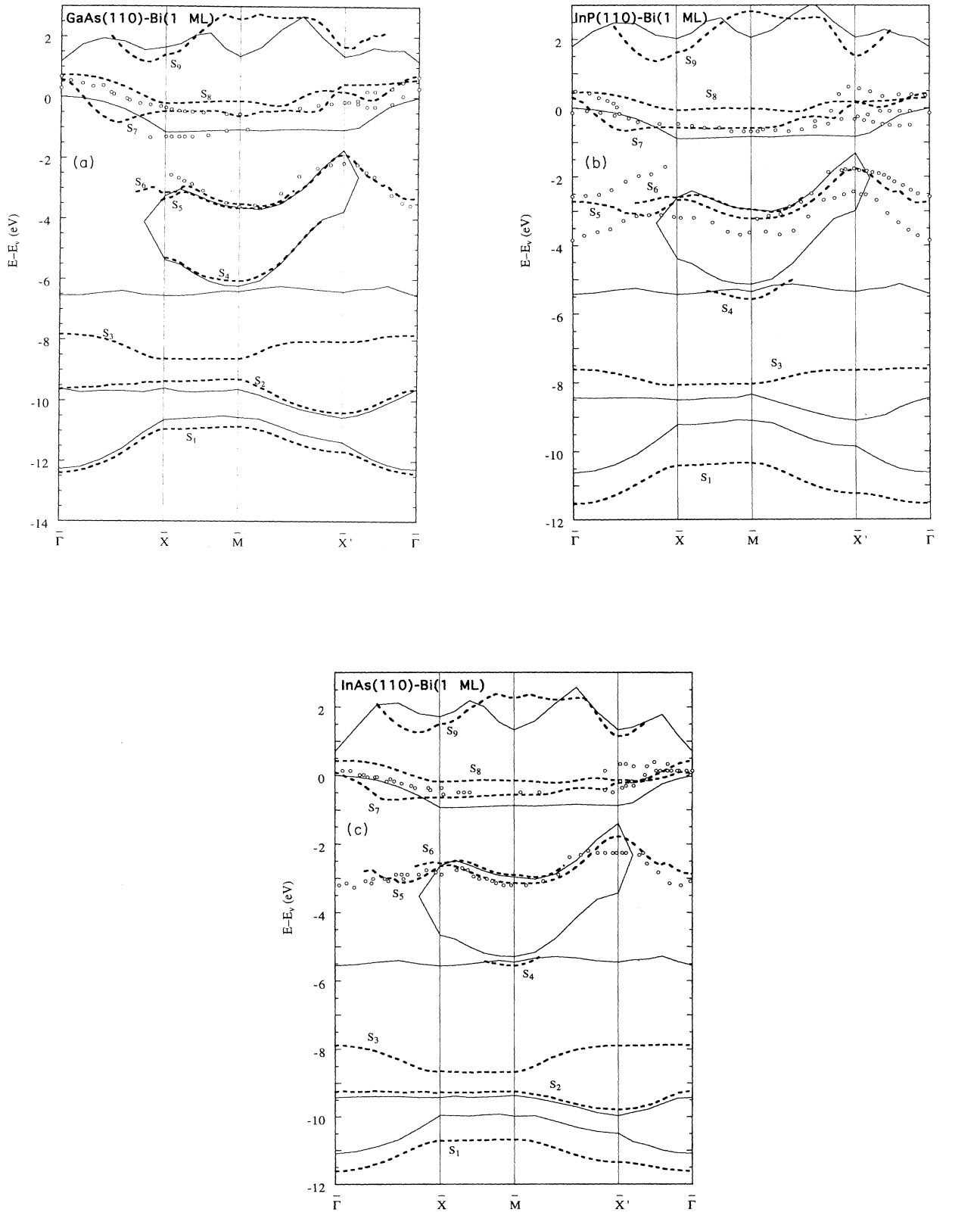

FIG. 4. Electronic band structure of an ordered monolayer of Bi on (a) GaAs(110), (b) InP(110), and (c) InAs(110). Projected bulk band regions are shown by solids lines, surface localized states are indicated by dashed lines, and angle-resolved data are indicated by open circles.

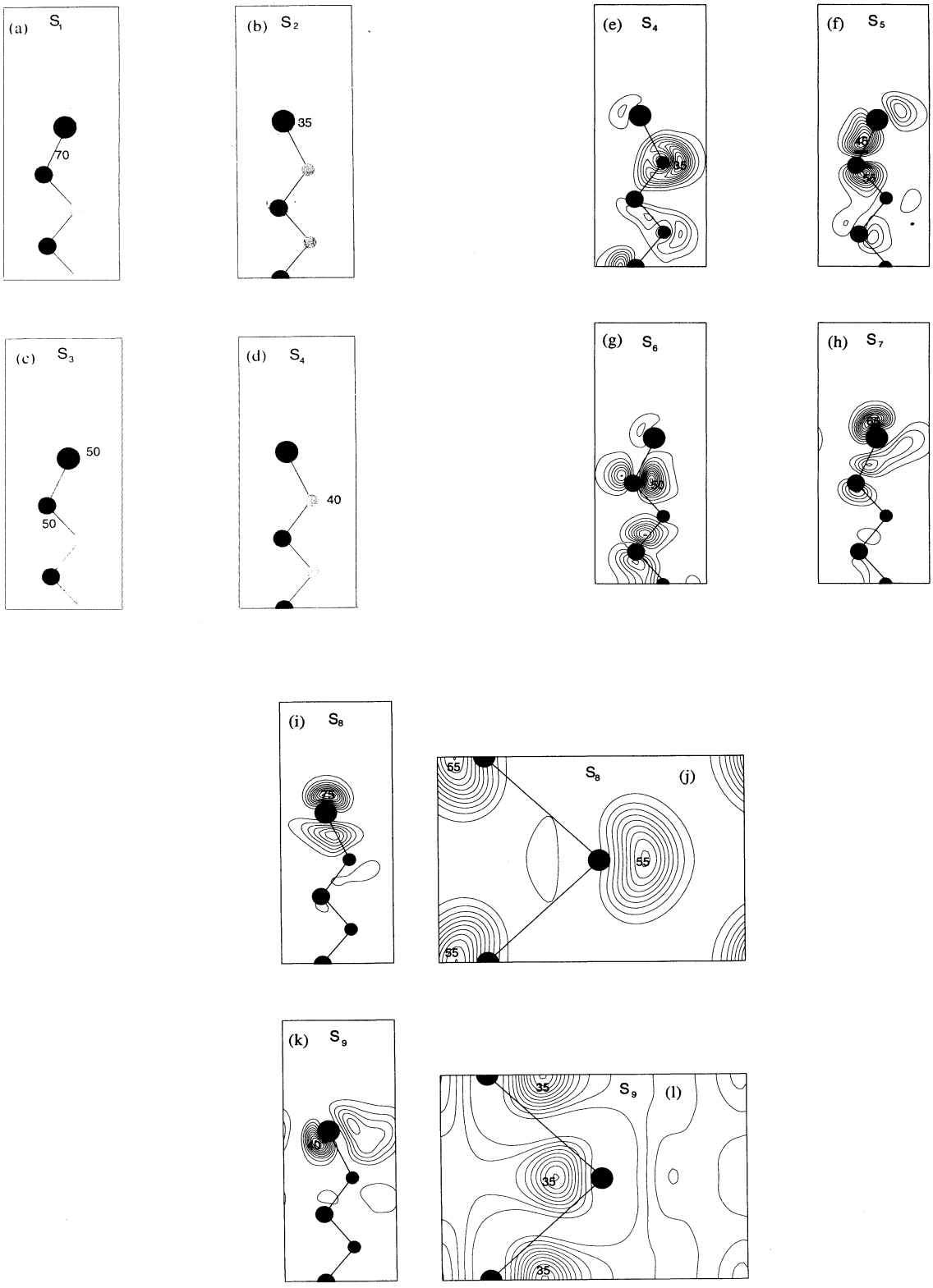

FIG. 5. Charge-density plots for selected interface states on InAs(110)-Bi(1 ML): (a) S_1 at $\bar{X}$, (b) S_2 at $\bar{X}$, (c) S_3 at $\bar{X}$, (d) S_4 at $\bar{M}$, (f) S_5 at $0.5(\bar{X}-\bar{M})$, (g) S_6 at $0.5(\bar{X}-\bar{M})$, (h) S_7 at $\bar{X}$, (i) S_8 at $\bar{X}$, (j) S_8 at $\bar{X}$, (k) S_9 at $\bar{X}$, (l) S_9 at $\bar{X}$. Also shown in (e) is S_4 for GaAs(110)-Bi(1 ML) at $\bar{M}$. The plots in (a)–(i), (k) are in the $(1\bar{1}0)$ plane, and the plots in (j) and (l) are in the (110) plane.

bonding combinations of the s orbitals of the overlayer and substrate anion atoms. This feature has also been observed[46] for InP(110)-Sb(1 ML).

The state S_4 is glimsed at the upper edge of the ionicity gap around $\bar{M}$ for the InP and InAs substrates, and along $\bar{X}$-$\bar{M}$-$\bar{X}'$ just inside the stomach gap for the GaAs substrate. In all three cases it is associated (somewhat weakly) with an orbital on the first substrate layer cation atom [see Fig. 5(d) and Fig. 5(e) for the cases of InAs(110)-Bi(1 ML) and GaAs(110)-Bi(1 ML) at $\bar{M}$, respectively].

S_5 and S_6 are two bands which skirt across the top of the stomach gap for each of our overlayer systems. For the InP substrate their maximum separation is fractionally greater than that of InAs and GaAs, which may explain why both bands have been experimentally observed only in this case, and single bands in the other cases. These bands are both related to p orbitals located on the 1st substrate layer anion atom, which may be another reason for the difficulty of experimentally distinguishing them. They are depicted in Fig. 5(f) and 5(g) for the case of InAs(110)-Bi(1 ML) at $0.5(\bar{X}$-$\bar{M})$. The state S_6 has a large contribution from the substrate anion p_y orbital and a small $p_\perp$ contribution from the Bi atom. The S_5 state has a large p_z contribution from the substrate anion and a small p contribution from Bi. These two bands cross at around $\bar{X}$, and, thus, to the left of $\bar{X}$ the substrate's p_y and p_z contributions are swapped. The bands S_5 and S_6 are nearly degenerate throughout $\bar{X}$-$\bar{M}$-$\bar{X}'$. Schmidt, Wenzien, and Bechstedt[12] have noted a similar situation for GaAs(110)-Sb(1 ML).

The second highest occupied state is S_7. It lies above the bulk valence-band edge everywhere except for part of $\bar{\Gamma}$-$\bar{X}$. In the region of $\bar{X}$, it is derived from a bonding configuration between a $p_\perp$ orbital on the cation Bi atom and a $p_\parallel$ wave function on its anion neighbor [see Fig. 5(h)]. Its character changes along $\bar{X}$-$\bar{M}$-$\bar{X}'$, and at $\bar{X}'$ is associated with interacting $p_\perp$ orbitals located on both types of Bi atoms.

The highest occupied state S_8 lies entirely above the valence-band edge, with relatively flat dispersion along $\bar{X}$-$\bar{M}$-$\bar{X}'$. In the region of $\bar{X}$, it is derived from a p_z dangling bond on the anion Bi atom, together with some interaction with its cation neighbor [see Fig. 5(i)]. This interpretation of the highest occupied state on III-V(110)-Bi(1 ML) is similar to that presented theoretically[11,13,46] for a monolayer of Sb. At $\bar{X}'$ this state is composed of p_z orbitals on both types of Bi atoms, forming an antibonding configuration of the type shown in Fig. 5(j). Our interpretation of this state is also in agreement with the finding from the experimental work of McLean *et al.*[47] for GaAs(110)-Sb(1 ML).

The lowest unoccupied state S_9 disappears into the bulk in the regions around $\bar{\Gamma}$ and $\bar{M}$, with a minimum at $0.8(\bar{\Gamma}$-$\bar{X})$ and a slightly higher lying minimum at $\bar{X}'$. At $\bar{X}$, this state is associated with an $sp_\perp$ orbital located on the anion Bi atom [see Fig. 5(k)], while at $\bar{X}'$ it is derived from a Bi-Bi antibonding chain of p_y orbitals [see Fig. 5(l)]. This state lies below the conduction-band edge in InP, but above the conduction-band edge in GaAs and InAs.

Photoemission measurements[4,44,45] have only been able to detect surface or overlayer states with low binding energies, typically up to 4 eV below the bulk valence-band edge. As seen from Fig. 4, these can be identified with the states S_5-S_8 obtained in our work. In the binding-energy range 2–3.5 eV, these measurements have produced two surface bands for Bi/InP, and only one surface band for Bi/GaAs and Bi/InAs. These can be compared with the nearly degenerate bands S_5 and S_6. In the energy range $+0.5$ eV to -1.0 eV, with reference to the bulk valence-band edge, photoemission measurements have mapped out two surface states. These show reasonable agreement with the states S_7 and S_8 of this work. A clear feature of the highest occupied state, from both experiment and theory, is that it shows very little dispersion along $\bar{X}$-$\bar{M}$-$\bar{X}'$. In addition, both experiment and theory identify two bands along $\bar{\Gamma}$-$\bar{X}'$, which cross and anticross.

The leading edge of S_8 lies at about 0.7 eV above the GaAs valence-band maximum, and about 0.5 eV above the valence-band maximum in InP or InAs, in agreement with photoemission measurements.[4,44] This energy edge can be regarded as the Fermi-level pinning position for p-doped substrate, and its position above bulk valence-band maximum provides a measure of the corresponding Schottky barrier height for the Bi covered system. The bonding character of this state, viz. the bonding between the p_z orbitals of the overlayer Bi and the substrate cation as discussed above, provides an understanding of the nature of Schottky barrier formation for p-doped substrate. The unoccupied dangling-bond nature of the state S_9 could pin the Fermi level for n-doped substrates. This state lies below the bulk conduction-band edge for the substrates GaAs and InP, but above it for InAs. The transition $S_8 \rightarrow S_9$ is indirect with magnitudes approximately 0.5, 0.8, and 0.7 eV for GaAs, InP, and InAs substrates, respectively.

IV. CONCLUSION

In conclusion, we have developed a robust method of solving the Kohn-Sham equations for both the electronic and geometric degrees of freedom within the pseudopotential approach and local-density approximation. We have applied this technique to study clean III-V(110) surfaces and III-V(110)-Bi(1 ML) systems. Our calculated equilibrium geometry agrees well with the results obtained from LEED analysis and a combination of XSW and SEXAFS determination. In addition, there is excellent agreement with previous Car-Parrinello type calculations. There is fairly good agreement between the calculated surface states and photoemission data. Similarly, the calculated atomic geometry for the ordered monolayer deposition of Bi on these surfaces is found to be in very good agreement with available results from XSW and LEED studies. The calculated electronic structures

of the overlayer systems show reasonable agreement with recent angle-resolved photoemission measurements. Our work also explains the orbital characters of the important adsorbate induced states in the substrate band gap, together with their role in Schottky barrier formation.

ACKNOWLEDGMENTS

One of us (A.U.) has been supported by the SERC, U.K. We also thank the SERC, U.K. for computational facilities through the CSI scheme.

*Present address: Department of Mathematics, City University, Northampton Square, London EC1V 0HB, U.K.

[1]F. McGilp and A. B. McLean, J. Phys. C **21**, 807 (1988).

[2]C. Stringer, A. McKinley, G. Hughes, and R. H. Williams, Vacuum **33**, 597 (1983); P. Mårtensson and R. M. Feenstra, Phys. Rev. B **39**, 7744 (1989); J. J. Joyce, M. M. Nelson, M. Tang, Y. Meng, J. Anderson, and G. J. Lapeyre, J. Vac. Sci. Technol. A **8**, 3542 (1990).

[3]P. Mårtensson, G. V. Hansson, M. Lähdeniemi, K. O. Magnusson, S. Wilkund, and J. M. Nicholls, Phys. Rev. B **33**, 7399 (1986); I. T. McGovern, R. Whittle, D. R. Zahn, C. Muller, C. Nowak, A. Cafolla, and W. Braun, J. Phys. Condens. Matter **3**, SA367 (1991).

[4]A. B. McLean, R. Ludeke, M. Prietsch, D. Heskett, D. Tang, and T. M. Wong, Phys. Rev. B **43**, 7243 (1991); A. B. McLean, R. M. Feenstra, A. Taleb-Ibrahimi, and R. Ludeke, *ibid.* **39**, 12 925 (1989).

[5]G. D. Waddill, C. M. Aldao, C. Capasso, P. J. Benning, Y. Hu, T. J. Wagener, M. B. Jost, and J. H. Weaver, Phys. Rev. B **41**, 5960 (1990).

[6]W. K. Ford, T. Guo, D. L. Lessor, and C. B. Duke, Phys. Rev. B **42**, 8952 (1990).

[7]W. K. Ford, T. Guo, K.-J. Wan, and C. B. Duke, Phys. Rev. B **45**, 11 896 (1992).

[8]T. Kendelewicz, J. C. Woicik, K. E. Miyano, A. Herrera-Gomez, P. L. Cowan, B. A. Karlin, C. E. Bouldin, P. Pianetta, and W. E. Spicer, Phys. Rev. B **46**, 7276 (1992); K. E. Miyano, T. Kendelewicz, J. C. Woicik, P. L. Cowan, C. E. Bouldin, B. A. Karlin, P. Pianetta, and W. E. Spicer, *ibid.* **46**, 6869 (1992).

[9]A. Herrera-Gómez, T. Kendelewicz, J. C. Woicik, K. E. Miyano, P. Pianetta, S. Southworth, P. L. Cowan, B. A. Karlin, and W. E. Spicer, J. Vac. Sci. Technol. A **11**, 2354 (1993).

[10]J. L. Alves, J. Hebenstreit, and M. Scheffler, Phys. Rev. B **44**, 6188 (1991).

[11]G. P. Srivastava, Phys. Rev. B **46**, 7300 (1992); **47**, 16 616 (1993); J. Phys. Condens. Matter **5**, 4695 (1993).

[12]W. G. Schmidt, B. Wenzien, and F. Bechstedt, Phys. Rev. B **49**, 4731 (1994); F. Bechstedt, W. G. Schmidt, and B. Wenzien, Europhys. Lett. **25**, 357 (1994).

[13]C. Mailhiot, C. B. Duke, and D. J. Chadi, Phys. Rev. B **31**, 2213 (1985).

[14]J. P. LaFemina, C. B. Duke, and C. Mailhiot, J. Vac. Sci. Technol. B **8**, 888 (1990).

[15]A. Umerski and G. P. Srivastava, Phys. Rev. B **48**, 8450 (1993).

[16]C. A. Swarts, W. A. Goddard, and T. C. McGill, J. Vac. Sci. Technol. **17**, 982 (1982).

[17]P. Skeath, C. Y. Su, W. A. Harrison, I. Lindau, and W. E. Spicer, Phys. Rev. B **27**, 6246 (1983).

[18]P. Mårtensson and R. M. Feenstra, Phys. Rev. B **39**, 7744 (1989); J. Microsc. **152**, 761 (1988).

[19]R. Car and M. Parrinello, Phys. Rev. Lett. **55**, 2471 (1985).

[20]P. Bendt and A. Zunger, Phys. Rev. Lett. **50**, 1684 (1983).

[21]P. Hohenberg and W. Kohn, Phys. Rev. **136**, B864 (1964); W. Kohn and L. J. Sham, *ibid.* Rev. **140**, A1133 (1965).

[22]G. P. Srivastava, J. Phys. A **17**, L317 (1984).

[23]D. M. Wood and A. Zunger, J. Phys. A **18**, 1343 (1985), and references therein.

[24]We have not found an overall saving of CPU if the first-order corrections to these eigenvectors are computed and used.

[25]We use this name, as **A** plays the same role as "preconditioning matrices" used in conjugate gradient algorithms designed for the solution of linear equations.

[26]J. Ihm, A. Zunger, and M. L. Cohen, J. Phys. C **12**, 4409 (1979).

[27]G. P. Srivastava and D. Weaire, Adv. Phys. **36**, 463 (1987).

[28]G. R. Walsh, *Methods of Optimization* (Wiley, New York, 1975).

[29]W. H. Press, B. P. Flannery, S. A. Teukolsky, and W. T. Vetterling, *Numerical Recipes* (Cambridge University Press, Cambridge, 1986).

[30]T. A. Arias, M. C. Payne, and J. D. Joannopoulos, Phys. Rev. B **45**, 1538 (1992).

[31]This generates overlayer geometry which is topologically equivalent to the Goddard geometry.

[32]We could have used theoretically predicted lattice constants (approximately 2% smaller than experiment), but this would have led to an artificial opening of band gap, creating confusion between the prediction of local-density approximation and experimentally measured values.

[33]G. B. Bachelet, D. R. Hamann, and M. Schlüter, Phys. Rev. B **26**, 4199 (1982).

[34]D. M. Ceperley and B. I. Alder, Phys. Rev. Lett. **45**, 566 (1980); J. P. Perdew and A. Zunger, Phys. Rev. B **23**, 5048 (1981).

[35]R. A. Evarestov and V. P. Smirnov, Phys. Status Solidi B **119**, 9 (1983).

[36]F. Bechstedt and R. Enderlin, *Semiconductor Surfaces and Interfaces* (Akademic, Berlin, 1988), and references therein.

[37]J. C. Woicik, T. Kendelewicz, K. E. Miyano, P. L. Cowan, B. A. Karlin, C. E. Bouldin, P. Pianetta, and W. E. Spicer, Phys. Rev. Lett. **68**, 341 (1992); J. C. Woicik, T. Kendelewicz, K. E. Miyano, M. Richter, C. E. Bouldin, P. Pianetta, and W. E. Spicer, Phys. Rev. B **46**, 9869 (1992).

[38]A. Huijser, J. van Laar, and T. L. van Rooy, Phys. Lett. **65A**, 337 (1978).

[39]L. Sorba, V. Hinkel, H. U. Middelmann, and K. Horn, Phys. Rev. B **36**, 8075 (1987).

[40]D. M. Swanson, A. B. McLean, D. N. McIlroy, D. Heskett, R. Ludeke, H. Munekata, M. Prietsch, and N. J. DiNardo, Surf. Sci. **312**, 361 (1994).

[41]The local-density approximation underestimates bulk and surface band gaps, but these can be corrected for by using a quasiparticle calculation, see, e.g., M. S. Hybertsen and S. G. Louie, Phys. Rev. B **34**, 5390 (1986); **38**, 4033 (1988); X. Zhu, S. B. Zhang, S. G. Louie, and M. L. Cohen, Phys. Rev. Lett. **63**, 2112 (1989).

[42]As already remarked, these valeus are subject to the usual band-gap underestimations due to the application of the local-density approximation. However, it should also be pointed out that the band-gap values reported here are ex-

pected to be reduced upon consideration of higher-energy cutoff for plane-wave expansion.

[43]H. Carstensen, R. Claessen, R. Manzke, and M. Skibowski, Phys. Rev. B **41**, 9880 (1990).

[44]R. Whittle, E. Dudzik, I. M. McGovern, D. R. T. Zahn, C. Nowak, A. Cafolla, and W. Braun, Surf. Sci. **287**, 554 (1993).

[45]D. N. McIlroy, D. Heskett, D. M. Swanston, A. B. McLean, R. Ludeke, H. Munekata, M. Prietsch, and N. J. DiNardo, Phys. Rev. B **47**, 3751 (1993).

[46]G. P. Srivastava and R. P. Martin, J. Phys. Condens. Matter **4**, 2009 (1992).

[47]A. B. McLean, R. Ludeke, M. Prietsch, D. Heskett, D. Tang, and T. M. Wong, Phys. Rev. B **43**, 7243 (1991).